RSC Advances

PAPER

View Article Online
View Journal | View Issue

Cite this: *RSC Adv.*, 2017, **7**, 47662

Bacterial cellulose–TiO_2 nanocomposites promote healing and tissue regeneration in burn mice model

Ayesha Khalid,[a] Hanif Ullah,[b] Mazhar Ul-Islam,[c] Romana Khan,[d] Shaukat Khan,[e] Fiaz Ahmad,[f] Taous Khan*[b] and Fazli Wahid *[a]

The development of novel cutaneous wound treatments particularly for burns is of paramount importance due to complex pathophysiology, prevalent infection and clinical complexities associated with burn care. The main focus of the current study was to investigate the *in vivo* burn wound healing potential of bacterial cellulose (BC) and titanium dioxide (TiO_2) nanocomposites (BC–TiO_2). The physicochemical characterization of BC–TiO_2 was carried out using FE-SEM, XRD and FT-IR. The antimicrobial activity of the nanocomposite was tested against *Escherichia coli* and *Staphylococcus aureus* through agar disc diffusion protocol. The *in vivo* wound healing efficacy was evaluated in burn wound model through wound area measurement, percent contraction and histopathology. The characterization results confirmed the successful incorporation of TiO_2 nanoparticles into BC. The nanocomposites exhibited 81 ± 0.4% and 83 ± 0% inhibition against *E. coli* and *S. aureus*, respectively. The composite bandage showed good healing pattern with 71 ± 2.41% wound contraction. Histopathological evidence like the formation of healthy granulation tissue and the re-epithelization indicated the healing progression in the composite treated group. In comparison, the BC treated group has partial epithelization and signs of inflammation. These results proved that the composite dressing possesses an excellent healing potential with faster re-epithelization rate and accelerated wound contraction ability and thus could be a candidate for the development of cutaneous wound care products to address the limitations of the conventional wound dressing for burns.

Received 15th June 2017
Accepted 24th September 2017

DOI: 10.1039/c7ra06699f

rsc.li/rsc-advances

1. Introduction

Bacterial cellulose (BC), a biopolymer produced by certain microbial genera, offers a wide range of applications in the field of tissue engineering, drug delivery,[1] biomedicines,[2] and chronic wound therapy.[3] BC has been widely investigated as a temporary skin substitute due to its effective water retaining capability, high porosity and biocompatibility.[4] This unique polymer possesses all of the features desired for an ideal wound care product.

Healing is a physiological curative consequence of any injury. Cutaneous wound healing is an intricate process, achieved through highly precise and programmed phases, synchronized to respond immediately after an injury. Wound healing follows a complex sequence of events at the cellular level, which replaces the devitalized tissues and restores the natural characteristics of the skin that are compromised by an injury.[5] The previous study revealed that the moist environment favours the autolytic debridement and enhances proteolytic activity and increases the rate of re-epithelization.[6] Thus, the accumulation of the growth factors and the extracellular matrix increases, which facilitates healing. Improper healing leads to chronic wounds. Therefore, in order to promote healing of chronic wounds, particularly burns, proper dressing material that can absorb exudates, reduce the pain and provide sterile environment for normal healing progression is required.[7]

The moist and hydrophilic nature of BC can provide an appropriate environment for healing. BC has a better ability to enhance the healing process of chronic wounds and burns compared to traditional dressings. BC not only provides optimal wound healing environment but also reduces pain and can conform to the wound surface particularly to facial contours due to its elastic and hydrophilic nature. Therefore, the hierarchical structure of BC films promotes the migration of cells and facilitates cutaneous healing.[8] Lack of inherent antimicrobial activity, however, limits the use of BC as a wound care material. Its modification by collagen, alginate, chitosan and different antimicrobial agents was carried out in order to

[a]*Biotechnology Program, COMSATS Institute of Information Technology, Abbottabad-22060, Pakistan. E-mail: fazliwahid@ciit.net.pk*

[b]*Department of Pharmacy, COMSATS Institute of Information Technology, Abbottabad-22060, Pakistan. E-mail: taouskhan@ciit.net.pk*

[c]*Department of Chemical Engineering, College of Engineering, Dhofar University, Salalah, Oman*

[d]*Department of Environmental Sciences, COMSATS Institute of Information Technology, Abbottabad-22060, Pakistan*

[e]*Department of Chemical Engineering, Kyungpook National University, Daegu, Korea*

[f]*Department of Pathology, Ayub Medical College, Abbottabad, Pakistan*

enhance the properties of BC.[9] For example, the BC and chitosan composite promoted better wound contraction and enhanced the epithelization compared with unmodified BC. In addition, this composite also possessed antibacterial activity against *E. coli* and *S. aureus*.[10] Similarly, BC and collagen-based hydrogel displayed promising results in this regard.[11] In another study, the composite of BC with vaccarin demonstrated an excellent healing potential and biocompatibility in rat skin model.[12] Despite these encouraging pre-clinical results, the search for an ideal skin repair material still continues.

In the current study, the effectiveness of BC as a wound dressing material has been improved by fabricating its composites with TiO_2 nanoparticles. The super-hydrophilic and photocatalytic properties, stable chemical nature, and biocompatibility of TiO_2 nanoparticles[13] make them an ideal candidate for cosmetic industry, particularly for manufacturing more innovative skin care products.[14] TiO_2 based nanostructured biomaterials have attracted much attention in the field of biomedical engineering, particularly in bone tissue engineering, nano TiO_2 bone scaffold, biosensors and manufacturing of vascular implants. The use of TiO_2 nanotubes for controlled drug delivery is a quite promising approach.[15] The wound healing activity of the synthesized composite bandage was assessed for deep partial thickness burns in mice model. The antibacterial activity of the designed composite was checked against two most prevalent pathogens of burn wounds, *i.e. Escherichia coli* (*E. coli*) and *Staphylococcus aureus* (*S. aureus*). The composite displayed a strong antibacterial activity against the selected pathogens. The histological analysis further confirms the tissue regeneration capability of BC–TiO_2 composites.

2. Results and discussion

2.1. Characterization of TiO_2 nanoparticles

The morphology and structural features of TiO_2 nanoparticles were confirmed through transmission electron microscopy (TEM) and X-ray diffraction (XRD). TEM image shown in Fig. 1a indicated the successful synthesis of TiO_2 nanoparticles, which are semi-spherical, non-agglomerated and well dispersed. XRD analysis further confirmed the synthesis of TiO_2 nanoparticles through the display of various crystalline peaks of TiO_2 nanoparticles as shown in Fig. 1b. The peaks at $2\theta = 25.30°$, 36.97°, 37.81°, 38.65°, 47.96°, 54.01°, 55.12°, 63.04°, 68.85°, 71.02° were assigned to the (101), (103), (004), (112), (200), (105), (211), (118), (116), and (220) planes of the anatase TiO_2, respectively.[16] The full width at half maximum (FWHM) values for all of the Miller indices ranged in 0.3–0.4°, while the crystallite size was in the range of 20–30 nm. The absence of the additional peaks in XRD spectrum confirmed the purity of the synthesized nanoparticles.

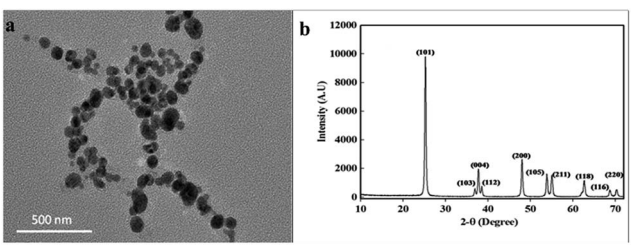

Fig. 1 (a) TEM image showed semi-spherical, non-agglomerated and well dispersed TiO_2 nanoparticles and (b) XRD pattern showed the planes of anatase TiO_2 nanoparticles.

2.2. Characterization of BC–TiO_2 nanocomposite

The morphology of BC and BC–TiO_2 composites was observed through field emission scanning electron microscopy (FE-SEM) microphotographs, which displayed a clear difference in BC and BC–TiO_2 composites. BC has an organized fibril network with plenty of empty spaces as shown in the cross section morphology in Fig. 2c. The SEM image of the composites (Fig. 2b) indicated that TiO_2 nanoparticles were attached to the surface of BC fibrils. A deep penetration of the nanoparticles into the BC matrix can also be observed from these microphotographs (Fig. 2d). The firm attachment of the nanoparticles on the surface fibril as well as the penetration inside the BC matrix ensure the negligible detachment during processing and treatment of the composites for various applications. The firmness was further confirmed from Ti^{4+} release experiments that resulted in less than 4 ppm of particles released in 10 days treatment (data are not included). These results are concurrent with our previous observations.[26] The distribution of TiO_2 nanoparticles is rather homogenous, which may indicate the pronounced mechanical, thermal, and biological properties of BC–TiO_2 composites.[17]

XRD analysis was conducted to investigate the crystalline properties of BC, and the synthesized BC–TiO_2 composites and the micro-structural changes in the BC sheets were caused by the impregnation of TiO_2 nanoparticles. The XRD patterns of the BC and BC–TiO_2 composites have been shown in Fig. 3. The semi-crystalline nature of BC has been primarily indicated by its broad crystalline peaks when analysed through XRD. BC usually

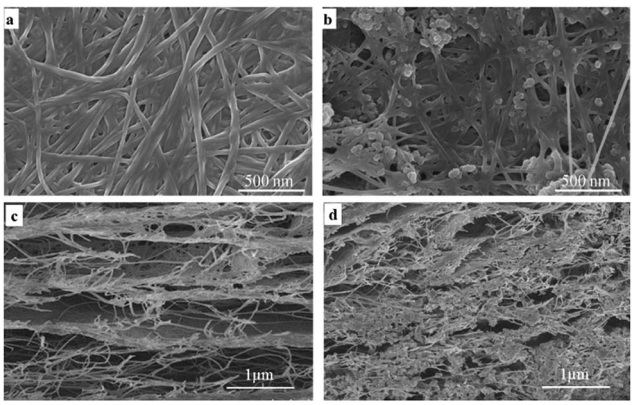

Fig. 2 SEM images of (a) the pure BC surface and (b) the BC–TiO_2 nanocomposites surface indicated the attachment of TiO_2 nanoparticles on BC fibrils surface and (c) the cross section of pure BC showing organized fibril network with plenty of empty spaces, while (d) the cross section of BC–TiO_2 nanocomposites showing the particles penetrated inside the BC matrix.

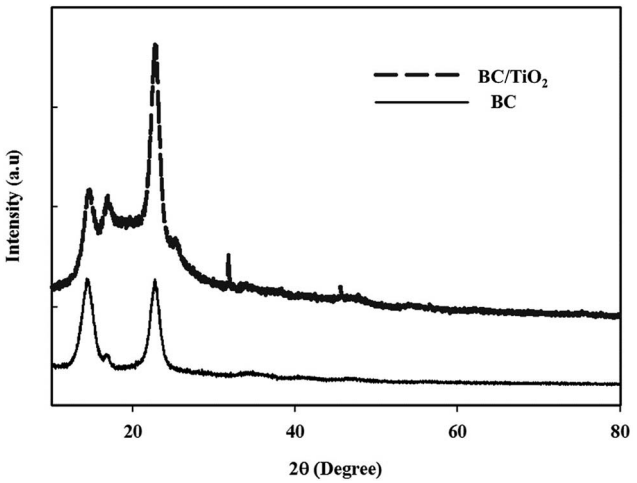

Fig. 3 XRD spectra show semi-crystalline nature of BC and BC–TiO_2 nanocomposites.

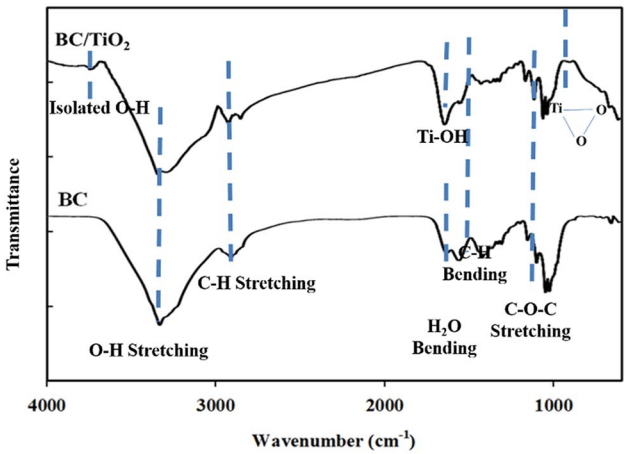

Fig. 4 FT-IR spectra showed the presence of fundamental peaks for various chemical groups in BC and BC–TiO_2 nanocomposites.

shows two major crystalline peaks around $2\theta \sim 14^\circ$ and ~22–23°,[18] which correspond to the crystallographic planes of $(1\bar{1}0)$, (110), and (200), respectively.[19] An amorphous halo at 2θ 19.6° represents the non-crystalline (amorphous) region of BC. The relative crystallinity of the pure BC and composite BC can be calculated from the relation of the peak at (200) with the amorphous peak.[20,21] If the TiO_2 particles are successfully impregnated in BC, the XRD patterns of the BC–TiO_2 composite must possess the diffraction peaks of both BC and TiO_2 nanoparticles. All of the characteristic peaks of BC as well as the prominent peaks of TiO_2 nanoparticles around 2θ 36° and 47° were present in the composites as shown in Fig. 3. It is obvious that some of the smaller peaks of TiO_2 did not appear in the spectra that might have been overlapped by or merged with the high amorphous region of BC. The peak intensity for BC was slightly lower in the composites that indicated a little decrease in the crystallinity. The relative crystallinity of BC was 65.4%, while it was only 53.8% for the BC–TiO_2 composites. This decreasing crystallinity trend agrees with some previous literatures, which have reported that the additives usually decrease the polymer crystallinity.[21,22]

Fourier transform infrared (FT-IR) spectra, shown in Fig. 4, depict the presence of all fundamental peaks for various chemical groups in BC. The broad characteristic peak for OH stretching is centred at 3350 cm^{-1}. A broader peak for biocellulose indicated a stronger hydrogen bonding between cellulose molecules.[18] Similarly, the peaks for CH stretching vibration were observed at 2890 cm^{-1} and this was further supported by the appearance of various peaks corresponding to CH bending vibrations at 1664 cm^{-1} and 1402 cm^{-1}. The peaks for the carbonyl group of glucose were obtained at 1678 cm^{-1}, while that for C–O–C stretching vibration appeared at 1060 cm^{-1}.[21] FT-IR spectra of the BC–TiO_2 contain all of the characteristics peaks of BC along with the additional peaks of TiO_2. A weak peak appearing around 3630 cm^{-1} could be attributed to the presence of free OH groups. The CH–O bending and C–O–C stretching peaks were suppressed in the spectra of BC–TiO_2 because of NPs attached on the BC surface. Instead, a strong peak for Ti–OH bending at 1635 cm^{-1} and a weak peak for peroxy triangular O–Ti–O could be observed. FT-IR spectra supported the results of FE-SEM and XRD.

2.3. Antibacterial assay

Microbial infection is a major factor that can lead to impaired wound healing. Therefore, the antimicrobial activity of the BC–TiO_2 nanocomposite was evaluated against the selected burn associated pathogens including *E. coli* and *S. aureus* (Fig. 5). Metal-based nanoparticles have been explored with significant inhibitory activity against a wide range of bacteria. Destruction of the cell wall and cell membrane integrity, enzyme inhibition and alteration of cellular mechanisms through reactive oxygen species (ROS) production are some of the general mechanisms through which nanoparticles induce death in bacterial cells.[23] The BC–TiO_2 nanocomposites showed 83 ± 0% inhibition against *S. aureus*, which is considered as the predominant pathogen in burn wound.[24] Similarly, it also exhibited 81 ± 0.4% inhibition against *E. coli* as shown in Table 1.

The current results are in accordance with the previous report where the antibacterial activity of TiO_2 nanoparticles was reported against a variety of microorganisms.[25] An artificial

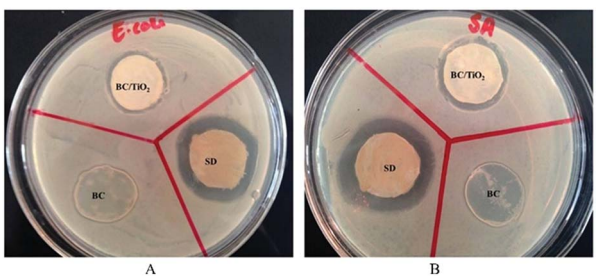

Fig. 5 Antibacterial activity of the BC–TiO_2 nanocomposites against (A) *E. coli* and (B) *S. aureus* through the disc diffusion assay. BC–TiO_2 nanocomposites showed prominent effects against the tested pathogens.

Table 1 The zone and percent inhibition of BC and BC–TiO_2 nanocomposites against selected pathogens through agar disc diffusion method

Bacterial specie	Zone of inhibition (mm)			Inhibition, %
	Standard drug	BC	BC–TiO_2	
E. coli	30 ± 0	0 ± 0	24.3 ± 0.5	81.0 ± 0.4
S. aureus	30.3 ± 0.5	0 ± 0	25 ± 0	83 ± 0

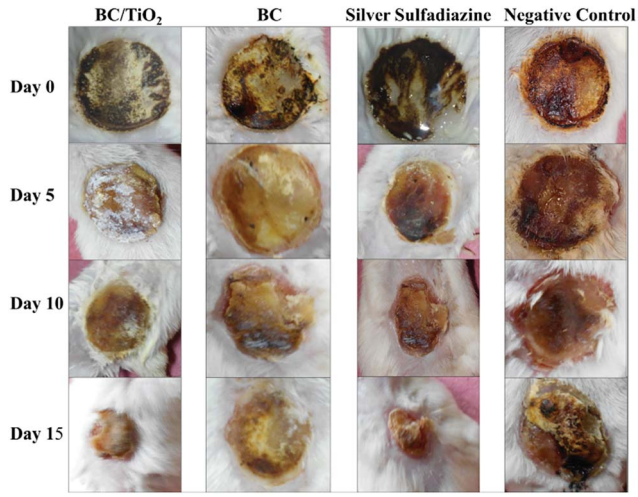

Fig. 6 Wound photographs of all treated groups including BC–TiO_2, BC, silver sulfadiazine and negative control groups on different treatment days. The prominent healing effects of BC–TiO_2 can be seen in comparison to simple BC group.

dressing composite fabricated with TiO_2 and poly lactic-*co*-glycolic acid (PLGA) also showed an effective antibacterial activity against *E. coli* and *S. aureus*.[15] It has been reported that the oxidative stress is the major factor responsible for bactericidal effects of the BC–TiO_2 nanocomposites.[26] The TiO_2 nanoparticles and the biocellulose/TiO_2 composite produce highly reactive species that destroy the lipopolysaccharides and peptidoglycan components of the cell membrane, thus, inducing cell death.[26] Increased rate of ROS production also alters the permeability of the mitochondrial membrane, which ultimately induces cell death. The destruction of peptidoglycan due to the direct contact of the cell with nanomaterials also decreases the viability of the bacterial cell.[1] Therefore, the BC–TiO_2 may have the same anti-bacterial mechanism against the tested pathogens. It is important to mention that BC alone did not show any activity against any tested strains, which is in agreement with the earlier reported literature.[27]

2.4. Wound healing activity of BC–TiO_2 nanocomposite

The wound healing activity of BC and BC–TiO_2 nanocomposite was periodically measured and photographed after 0, 5, 10 and 15 days. The photographs are shown in Fig. 6. It can be clearly seen in the photographs that the BC–TiO_2 composite and silver sulfadiazine (SD) treated groups have accelerated the wound closure compared to the pure BC and negative control groups. Wound area measured on respective days is given in Table 2. In all animals, the wound area on day 0 was 289 mm^2. A substantial decrease in the wound area was observed in the BC–TiO_2 nanocomposite treated group where it reduced to 236 mm^2 on day 5 and reached 86 mm^2 on day 15. In the BC treated group, the wound bed area decreased to 147.3 mm^2, while in the negative group, it just reduced to 248.3 mm^2 on day 15.

These findings clearly indicate that the incorporation of nanoparticles in BC significantly improved its healing potential. Physical contraction of the wound is presumably due to the activity of contractile fibroblasts, which is a critical feature of remodeling phase. Remodeling phase of wound healing may last for several years, where collagen producing fibroblasts along with other components of extracellular matrix (ECM) increase the tensile strength of the tissue so that its original architecture can be maintained.[28] The wound area was notably reduced in the BC–TiO_2 nanocomposite treated group, which may be due to the enhancement of fibroblasts functions.

2.4.1. Histopathology. Histological analysis is a powerful method to observe the progress in healing and tissue regeneration of wounds. The previous study demonstrated that during the proliferative phase of wound healing, fibroblasts and epithelial cells are the most dominant cells of the granulation tissue.[28] The haematoxylin and eosin (H&E) stained images, shown in Fig. 7a, revealed that the re-epithelization was in progress in the BC–TiO_2 nanocomposite treated group. The fibroblast and epithelial cells in the regenerated epithelium could be seen, while the presence of small blood vessels indicated the process of angiogenesis. Images of the negative group showed necrotic cells and dead slough with no signs of healing (Fig. 7d). On the other hand, inflammation reached up to subcutaneous muscle in the BC treated group but re-epithelization occurred simultaneously (Fig. 7b). The SD

Table 2 Average wound area during the course of treatment in the BC, BC–TiO_2 nanocomposites, negative and SD groups. $p \leq 0.05$ was considered statistically significant

Groups	Wound area measurement (mm^2) and percent healing (%)			
	Day 0	Day 5	Day 10	Day 15
BC–TiO_2	289 ± 0	236.0 ± 3.4***	163.3 ± 2.8***	86.0 ± 3.4***
Bacterial cellulose	289 ± 0	347.3 ± 4.6	275 ± 3	147.3 ± 3.0
Negative control	289 ± 0	343.3 ± 5.7	313.3 ± 5.7	248.3 ± 2.8
Silver sulfadiazine (SD)	289 ± 0	286.00 ± 1.73	145.0 ± 8.6	76.6 ± 5.7

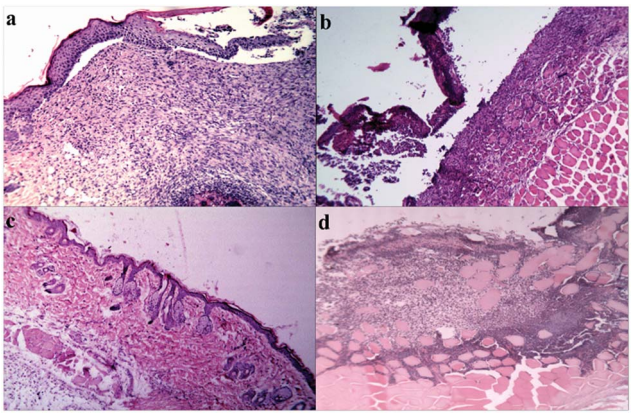

Fig. 7 H&E stained representative microphotographs of the treated wound tissue (a) BC–TiO_2, (b) BC, (c) positive control, and (d) negative control. The BC–TiO_2 treated group showed signs of proper healing progression as fibroblasts, epithelial cells and small blood vessels can be seen in the regenerated epithelium.

group also indicated the proper healing mechanism (Fig. 7c). The wound healing activity of TiO_2 nanoparticles engineered from a plant *Origanum vulgare* has also been reported in Wistar Albino rats.[29] The biocompatibility and anticoagulant properties of TiO_2 nanoparticles make them an excellent candidate for wound healing as observed in *in vitro* and *in vivo* studies.[15] The results of TiO_2-based scaffolds revealed the accelerated adhesion, proliferation and differentiation of osteoblasts, and ingrowth of vascular tissues.[15] Recently, a biocomposite comprised of a bilayer of TiO_2 and chitosan along with the extracellular matrix showed good wound healing properties *in vivo*.[30] A composite composed of chitosan and poly *N*-vinylpyrrolidone with a blend of TiO_2 nanoparticles showed an accelerated healing of open excision wounds in albino rats compared to the conventional gauze, soframycin skin ointment and chitosan.[31] Some studies also suggested that TiO_2 nanoparticles are very less toxic compared to other nanoparticles like carbon nanotubes and silicon dioxide.[32] It can be suggested from the current results (Fig. 7a) that the BC–TiO_2 nanocomposite treatment promotes appropriate healing through the fibroblast migration and proper development of epithelial cells along with the restoration of blood supply through the formation of new blood vessels.

3. Experimental

3.1. Materials

Titanium tetrachloride ($TiCl_4$), anhydrous benzyl alcohol ($C_6H_5CH_2OH$), glucose, sodium hydroxide (NaOH), osmium tetraoxide (OsO_4), phosphate buffer saline (PBS), glutaraldehyde, succinic acid and acetic acid were purchased from Sigma Aldrich Chemicals Company, St Louis, MO, USA. Bacteriological peptone and nutrient agar were supplied by Oxoid Ltd. Dextrose was purchased from Daejung, Korea. Sodium dihydrogen phosphate was obtained from Merck, Darmstadt, Germany, yeast extract powder was from HiMedia Laboratories Mumbai, India, and citric acid was from Riedel-deHaen, Germany.

3.2. Synthesis of TiO_2 nanoparticles

For the synthesis of TiO_2 nanoparticles, 80 ml of benzyl alcohol was placed in a pre-dried, two-necked flask followed by a dropwise addition of $TiCl_4$ under nitrogen flow as reported previously.[33] The mixture was heated to 80 °C and stirred for 24 h. The resultant white suspension was isolated and washed repeatedly with water and ethanol, followed by calcination at 600 °C for 1 h.[26]

3.3. Production of bacterial cellulose films

Gluconacetobacter xylinum (ATCC 53582) strain was used for the production of BC films. Hestrin Scharmm (HS) medium composed of 2% glucose, 0.5% yeast extract, 0.5% peptone, 0.27% Na_2HPO_4 and 0.115% acetic acid was used as a culture medium. HS agar plates containing 1.5% agar in addition to HS medium were used to spread the culture and incubated at 30 °C until the colonies appeared. These colonies of *G. xylinum* were inoculated into a 50 ml HS medium at 200 rpm orbital shaking incubator (WY 100) and at 30 °C for 24 h.

After this, 300 ml HS medium was poured into rectangular plastic containers along with 25 ml preculture and placed under static conditions at 30 °C for 7 days. The synthesized BC films were then washed with double distilled water and sterilized in an autoclave using 3 M NaOH at 150 °C for 15 min. The BC films were thoroughly washed with distilled water until neutral pH and stored in distilled water at 4 °C prior to use.[34]

3.4. Preparation of BC–TiO_2 nanocomposites

The BC–TiO_2 nanocomposites were prepared by impregnating the BC sheets in 1% aqueous suspension of TiO_2 nanoparticles in shaking incubator at 50 °C and 150 rpm for 24 h. The resulting BC–TiO_2 nanocomposites were used for wound treatment in wet form while they were freeze-dried (TELSTAR CRYODOS −50) at −50 °C for 10 h for physicochemical characterization.

3.5. Characterization of the TiO_2 nanoparticles and BC–TiO_2 nanocomposites

TEM and XRD were used to confirm the synthesis of the nanoparticles. The size of TiO_2 nanoparticles was calculated from an average of 30 nanoparticles through Image J software from TEM images. FE-SEM, XRD and FT-IR were used for the physicochemical characterization of TiO_2 nanocomposites. For TEM images, TiO_2 nanoparticles were well dispersed, and a drop of a dilute dispersion was put on a copper grid covered with a formal-carbon membrane. FE-SEM images of the freeze-dried BC and BC–TiO_2 nanocomposites were obtained using a Hitachi S-4800 and EDX-350 (Horiba) system (Tokyo Japan). The samples were fixed onto a brass holder and coated with osmium tetroxide (OsO_4) by a VD HPC-ISW osmium coater (Tokyo Japan) prior to FE-SEM observation. XRD patterns of the nanoparticles and nanocomposite were recorded on an X-ray diffractometer (X'Pert-APD PHILIPS, Netherland) with Cu Kα radiation with a wavelength of 1.54 Å. The X-ray generator tension and current were 40 kV and 30 mA, respectively. The

angle of scanning was varied in the range 10–70°. FT-IR spectra of the dried BC and nanocomposites were recorded with a Perkin Elmer FT-IR spectrophotometer (Spectrum GX & Autoimage, USA, Spectral range: 4000–400 cm^{-1}; Beam splitter: Ge coated on KBr; Detector: DTGS; Resolution: 0.25 cm^{-1} (step selectable)).

3.6. Antimicrobial assay of BC–TiO_2 composite films

The antimicrobial activity of the nanocomposites was evaluated against two most common burn wound pathogens *E. coli* and *S. aureus* through the agar disc diffusion assay.[34] The BC–TiO_2 composites and BC films were cut into 20 mm discs. Silver sulfadiazine cream was also coated on 20 mm discs of the sterilized filter paper and used as a positive control. Agar plates containing the lawn of the selected pathogens along with the discs were incubated at 37 °C for 24 h. After that, the zone of inhibition was measured. The antimicrobial potential of the composite was then determined through percent inhibition.

$$\text{Percent inhibition} = \left(\frac{\text{zone of inhibition of test sample (mm)}}{\text{zone of inhibition of standard drug (mm)}}\right) \times 100$$

3.7. Wound healing activity

3.7.1. Burn experimental model. The wound healing efficiency of the BC–TiO_2 nanocomposite was investigated using $BALB^c$ burn mice model. Initially, 20 animals were taken, weighed and divided into 4 groups with 5 animals in each group. The animals were purchased from National Institute of Health, Islamabad, Pakistan. The current study was performed according to the NIH guidelines for the care and use of laboratory animals (NIH Publication 1985 & 2011) and approved by the Institutional Ethics Committee for Animal Care and Use of COMSATS Institute of Information Technology (Abbottabad, Pakistan). The animals were kept in separate cages under a standard light–dark cycle and had free access to water and a balanced diet. Before induction of thermal injuries, the animals were sedated through intraperitoneal injection of 100 mg kg^{-1} ketamine and 10 mg kg^{-1} xylazine.[35] A commercial hair removing cream was used to remove the hairs from a selected area and then partial thickness burn wounds were induced through a metal bar heated on an open flame, which was applied perpendicularly to the designated area with gravitational pressure for 9 s. Analgesia and sedation were administered immediately after the procedure in order to ensure comfort and pain-free healing of the animals.

3.7.2. Treatment. After wound infliction, the BC–TiO_2 group was treated with 3 cm^2 piece of wet BC-nanocomposite as a bandage while the BC group was treated with unmodified BC. Topically applied silver sulfadiazine (SD) treated group was taken as the positive control, while the negative control group was left untreated. Disposable skin stapler (Ningbo Advan Electrical Co., Ltd, China) was used to fix the bandage on burn lesion. Treatment was continued for 15 days and the bandage was only changed on the 5th and 10th day. The area of the wound was measured on the 0, 5th, 10th and 15th day of the experiment, and the photographs were taken through a digital camera (Nikon S2900, Japan). Percent wound healing in all groups was calculated using the following formula.

$$\text{Percent healing} = 1 - \frac{\text{wound area on corresponding days}}{\text{wound area on day zero}} \times 100$$

3.7.3. Histological analysis. On day 15 of the experiment, all animals were sacrificed by cervical dislocation. Wound area tissues were surgically removed and stored in 10% formalin for histological analysis. Tissues were first fixed in 15% formalin and then 15% alcoholic formaldehyde. The dehydration of tissues was carried out by treating with 70%, 80% and absolute alcohol for 2, 3 and 6 h, respectively. Xylene solution was used for clearing and tissues were embedded in paraffin wax. The slides were prepared after cutting tissues with a microtome (Thermo Fisher Scientific, Germany) and stained with hematoxylin and eosin (H & E) dye. The prepared slides were then used for microscopic analysis to determine the healing and tissue regeneration.

3.8. Statistical analysis

The obtained data were expressed as mean ± standard deviation, while statistical analysis was carried out using Student's *t*-test through SigmaPlot. $p \leq 0.05$ was considered statistically significant (*represents significant statistical differences: $p \leq 0.001$***, $p \leq 0.01$**, $p \leq 0.05$*).

4. Conclusions

In recent years, intensive investigations have been carried out to develop innovative strategies for the effective antimicrobial dressings for a better management of chronic wounds. Besides all of the ideal properties of BC, lack of the inherent antimicrobial activity limits its use for clinical applications. Our findings have clearly demonstrated that the BC–TiO_2 nanocomposites possess an antibacterial activity. The accelerated healing progression in the composite treated animals, compared with that in the pure polymer treated group, has further confirmed that the composite dressing provides a sterile and favourable environment for skin repair. The potential therapeutic effects of this dressing can provide a base for developing clinically approved wound care products after toxicological analysis.

Conflicts of interest

There are no conflicts to declare.

Acknowledgements

This study was supported by the Higher Education Commission of Pakistan under Start-Up Research Grant Program (SRGP) (Grant No. 21-211/SRGP/R&D/HEC/2014).

References

1 H. Ullah, H. A. Santos and T. Khan, *Cellulose*, 2016, **23**(4), 2291–2314, DOI: 10.1016/j.carbpol.2010.10.072.
2 J. M. Rajwade, K. M. Paknikar and J. V. Kumbhar, *Appl. Microbiol. Biotechnol.*, 2015, **99**(6), 2491–2511.
3 S. P. Lin, I. L. Calvar, J. M. Catchmark, J. R. Liu, A. Demirci and K. C. Cheng, *Cellulose*, 2013, **20**(5), 2191–2219.
4 M. M. Abeer, M. Amin, M. C. Iqbal and C. Martin, *J. Pharm. Pharmacol.*, 2014, **66**(8), 1047–1061.
5 S. A. Guo and L. A. DiPietro, *J. Dent. Res.*, 2010, **89**(3), 219–229.
6 G. D. Winter, *Nature*, 1962, **193**(4812), 293–294.
7 S. Dhivya, V. V. Padma and E. Santhini, *Biomedicine*, 2015, **5**(4), 22.
8 W. K. Czaja, D. J. Young, M. Kawecki and R. M. Brown, *Biomacromolecules*, 2007, **8**(1), 1–2.
9 L. Fu, J. Zhang and G. Yang, *Carbohydr. Polym.*, 2013, **92**(2), 1432–1442, DOI: 10.1016/j.carbpol.2012.10.071.
10 S. P. Lin, I. L. Calvar, J. M. Catchmark, J. R. Liu, A. Demirci and K. C. Cheng, *Cellulose*, 2013, **20**(5), 2191–2219.
11 P. R. Moraes, S. Saska, H. Barud, L. R. Lima, V. D. Martins, A. M. Plepis, S. J. Ribeiro and A. M. Gaspar, *Mater. Res.*, 2016, **19**(1), 106.
12 Y. Qiu, L. Qiu, J. Cui and Q. Wei, *Mater. Sci. Eng., C*, 2016, **59**, 303–309, DOI: 10.1016/j.carbpol.2007.07.025.
13 A. Fujishima, T. N. Rao and D. A. Tryk, *J. Photochem. Photobiol., C*, 2000, **1**(1), 1–21.
14 A. Jaroenworaluck, W. Sunsaneeyametha, N. Kosachan and R. Stevens, *Surf. Interface Anal.*, 2006, **38**(4), 473–477.
15 J. Y. Wu, C. W. Li, C. H. Tsai, C. W. Chou, D. R. Chen and G. J. Wang, *Nanomed. Nanotech. Biol. Med.*, 2014, **10**(5), 1097–1107.
16 L. Zhao, H. Wang, K. Huo, L. Cui, W. Zhang, H. Ni, Y. Zhang, Z. Wu and P. K. Chu, *Biomaterials*, 2011, **32**(24), 5706–5716, DOI: 10.1016/j.biomaterials.2011.04.040.
17 M. Ul-Islam, W. A. Khattak, M. W. Ullah, S. Khan and J. K. Park, *Cellulose*, 2014, **21**(1), 433–447, DOI: 10.1016/j.carbpol.2012.03.093.
18 M. Ul-Islam, T. Khan and J. K. Park, *Carbohydr. Polym.*, 2012, **89**(4), 1189–1197.
19 C. Castro, R. Zuluaga, J. L. Putaux, G. Caro, I. Mondragon and P. Ganán, *Carbohydr. Polym.*, 2011, **84**(1), 96–102.
20 B. Focher, M. T. Palma, M. Canetti, G. Torri, C. Cosentino and G. Gastaldi, *Ind. Crops Prod.*, 2001, **13**(3), 193–208.
21 M. Ul-Islam, N. Shah, J. H. Ha and J. K. Park, *Korean J. Chem. Eng.*, 2011, **28**(8), 1736–1743.
22 M. Phisalaphong and N. Jatupaiboon, *Carbohydr. Polym.*, 2008, **74**(3), 482–488.
23 S. Galdiero, A. Falanga, M. Vitiello, M. Cantisani, V. Marra and M. Galdiero, *Molecules*, 2011, **16**(10), 8894–8918, DOI: 10.1016/S1389-5567(00)00002-2.
24 D. Church, S. Elsayed, O. Reid, B. Winston and R. Lindsay, *Clin. Microbiol. Rev.*, 2006, **19**(2), 403–434.
25 Q. Qin, J. Li and J. Wang, *Water Environ. Res.*, 2017, **89**(4), 378–383.
26 S. Khan, M. Ul-Islam, W. A. Khattak, M. W. Ullah and J. K. Park, *Cellulose*, 2015, **22**(1), 565–579.
27 T. Maneerung, S. Tokura and R. Rujiravanit, *Carbohydr. Polym.*, 2008, **72**(1), 43–51.
28 A. Gosain and L. A. DiPietro, *World J. Surg.*, 2004, **28**(3), 321–326.
29 R. Sankar, R. Dhivya, K. S. Shivashangari and V. Ravikumar, *J. Mater. Sci.: Mater. Med.*, 2014, **25**(7), 1701–1708.
30 C. H. Woo, Y. C. Choi, J. S. Choi, H. Y. Lee and Y. W. Cho, *J. Biomater. Sci., Polym. Ed.*, 2015, **26**(13), 841–854.
31 D. Archana, B. K. Singh, J. Dutta and P. K. Dutta, *Carbohydr. Polym.*, 2013, **95**(1), 530–539.
32 K. F. Soto, A. Carrasco, T. G. Powell, K. M. Garza and L. E. Murr, *J. Nanopart. Res.*, 2005, **7**(2), 145–169.
33 M. Niederberger, M. H. Bartl and G. D. Stucky, *Chem. Mater.*, 2002, **14**(10), 4364–4370.
34 A. Khalid, R. Khan, M. Ul-Islam, T. Khan and F. Wahid, *Carbohydr. Polym.*, 2017, **164**, 214–221.
35 P. A. Flecknell, *Br. J. Anaesth.*, 1993, **71**(6), 885–894.